JOURNAL OF GEOPHYSICAL RESEARCH, VOL. 104, NO. D17, PAGES 21,751–21,765, SEPTEMBER 20, 1999

Characteristics of marine boundary layers during two Lagrangian measurement periods 1. General conditions and mean characteristics

Qing Wang,[1] Karsten Suhre,[2] Paul Krummel,[3] Steve Siems,[4] Linlin Pan,[1] Timothy S. Bates,[5] James E. Johnson,[5] Donald H. Lenschow,[6] Barry J. Heubert,[7] Gregory L. Kok,[8] Richard D. Schillawski,[8] Andre S. H. Prévot,[8] and Steven Businger[7]

Abstract. Two sets of Lagrangian measurements were made during the southern Aerosol Characterization Experiment (ACE1) south of Tasmania, Australia, in December 1995. This paper intends to provide an overview of the general conditions encountered during the two intensive observational periods. The measurements by the NCAR C-130 provide the main data set for this study. We also use the sea surface temperature obtained from the R/V *Discoverer* and the European Centre for Medium-Range Weather Forecasts (ECMWF) analyses field for the large-scale divergence field. Emphases of the paper are on the atmospheric and oceanic environment and the boundary layer mean structure during the six flights in the two Lagrangian measurement periods. The large scale features, such as variations of sea surface temperature, synoptic conditions, and large-scale velocity fields, are discussed. These large-scale environments had significant influences on boundary layer turbulence and the inversion structure. The boundary layer mean structure and its evolution along the Lagrangian trajectory are also studied using two-dimensional cross-section plots of vertical and horizontal (along the flight track) variation of potential temperature, water vapor, wind components, and ozone concentration. The most prominent feature of the boundary layer is the two-layered structure observed throughout Lagrangian B and during the last flight of Lagrangian A. The two layers have detectable differences in potential temperature, water vapor, and, to a lesser extent, ozone concentration. These differences make it necessary to study the exchange between the two layers. Low-level cloud structure and cloud microphysics are also discussed. We emphasize, though, that the results on cloud fractions should be used with caution due to the variable nature of the cloud bands observed during ACE1.

1. Introduction

The Southern Hemisphere Marine Aerosol Characterization Experiment (ACE1) was conducted from November 15 to December 14, 1995 [*Bates et al.*, 1998]. The primary measurement area was south of Tasmania, Australia, over the southern Pacific Ocean. During ACE1, coordinated measurements were made by a research aircraft, the C-130, operated by the National Center for Atmospheric Research (NCAR), and a NOAA research vessel *Discoverer*. These efforts resulted in two successful Lagrangian intensive observational periods (hereinafter referred to as Lagrangians) where a tagged air column was traced and sampled for 2 days during each Lagrangian. This study focuses on the large-scale condition and the boundary layer mean structure observed during these two Lagrangians.

The philosophy of Lagrangian measurements has been discussed by *Bretherton et al.* [1995] and *Huebert et al.* [1996]. The strategy is to make measurements following the same air column for an extensive period. During each Lagrangian, the selected air column was tagged by constant-level balloons that radioed their positions to the C-130 [*Businger et al.*, 1998]. There are two major advantages of this measurement strategy: (1) by measuring the time rate of change of aerosol and trace gas concentration, the hard-to-measure terms, such as the source and sink terms, can be obtained from the aerosol budget equation; and (2) by following the same air column, the time rate of change of a quantity following a parcel or a column of air (the total derivative) is measured directly. It is therefore unnecessary to consider the effects of horizontal advection. The Lagrangian

[1]Meteorology Department, Naval Postgraduate School, Monterey, California.
[2]Laboratorie d'Aérologie, UMR CNRS/UPS, Toulouse, France.
[3]CSIRO Division of Atmospheric Research, Aspendale, Victoria, Australia.
[4]Department of Mathematics, Monash University, Clayton, Victoria, Australia.
[5]Pacific Marine Environmental Laboratory, NOAA, Seattle, Washington.
[6]Mesoscale and Microscale Meteorology Division, NCAR, Boulder, Colorado.
[7]Department of Oceanography, University of Hawaii, Honolulu, Hawaii.
[8]Research Aviation Facility, NCAR, Boulder, Colorado.

Paper number 1998JD100099.
0148-0227/99/1998JD100099$09.00

measurement strategy was first successfully implemented during the Atlantic Stratocumulus Transition Experiment/Marine Aerosol and Gas Experiment (ASTEX/MAGE). Results from ASTEX/MAGE showed that this measurement strategy could provide an integrated data set for understanding the evolution of boundary layer clouds and aerosol chemistry [e.g., *Zhuang and Huebert*, 1996; *Bretherton et al.*, 1995; *Wang*, 1995; *DE Roode and Duynkerke*, 1996].

This is the first of two papers describing the characteristics of the boundary layer mean and turbulence structure during the two Lagrangian intensive observational periods (IOP). This paper focuses on mean vertical structure and the surface and large-scale forcing on the boundary layer. *Wang et al.* [this issue] will focus on the boundary layer turbulence and entrainment characteristics. The primary data used in this study were obtained by the NCAR C-130 and the R/V *Discoverer*. Analyses from the European Centre for Medium-Range Weather Forecasts (ECMWF) will also be used to provide the large-scale environmental conditions. Section 2 provides an overview of the two Lagrangian measurements. Section 3 discusses the general synoptic conditions and air mass interactions. Section 4 discusses the variation of sea surface temperature observed from the C-130 and the R/V *Discoverer*. Discussions of the evolution of boundary layer mean thermodynamic structure are given in section 5. Cloud characteristics and microphysics will be given in section 6. The inversion structure and the effects of large-scale forcing will be discussed in section 7. The effects of variations in boundary layer wind on the Lagrangian measurement will be discussed in section 8. The results are summarized in section 9.

2. Coordinated Measurements During Lagrangians A and B

Two Lagrangian IOPs were made by the NCAR C-130 in early December 1995 during ACE1. The first Lagrangian (Lagrangian A, hereinafter referred to as LA) was made on December, 1 and 2 and the second (Lagrangian B (LB)) on December 7 and 8. Each Lagrangian contained three research flights.

A circular flight pattern was flown by the NCAR C-130 for the first time in ACE1. This flight pattern had longer measurement duration at each altitude compared to the conventional L-shaped flight pattern, which should result in higher confidence in the turbulence statistics. The circular legs also provided an estimate of the large-scale divergence/convergence from the mean wind measurements [*Lenschow*, 1996]. Usually, circles approximately 60 km in diameter were flown at four levels in the boundary layer and one level above. Adjacent circles were flown in opposite directions (clockwise or counterclockwise) in order to cancel out the uncertainties in the retrieved horizontal velocity as the result of a nonzero bias in airspeed and sideslip angle. The divergence calculation and a thorough evaluation of this measurement technique are discussed by *Lenschow* [1996]. A three-dimensional view of a typical flight pattern is shown in Figure 1. It is noted here that the circles were not "closed" if viewed from a fixed coordinate since the C-130 drifted with the mean wind at the measurement level. A "perfect" circle can be obtained if the drift by the mean wind was subtracted from the trajectory. Depending on the time available for measurements, usually two to three vertical stacks of circular legs were flown during each flight.

In addition to the level circular legs, several aircraft soundings were also made during each flight. At the boundary layer top, at least one flight leg that went in and out of the boundary layer in a porpoise maneuver was also made to sample the inversion structures. These aircraft measurements provided the main data set for this study. Two downward looking lidar legs across the diameter of the circle were also flown before and after the stacks of circles and soundings to study aerosol back scattering in the measurement area. A general description of the coordinated efforts between the R/V *Discoverer* and the C-130 during each Lagrangian is given below.

2.1. Lagrangian A

Lagrangian A was initiated with the launch of a "smart" balloon from R/V *Discoverer* at 1245 (UTC), December 1, located at 45°S, 141°E. The balloon was released in a mostly clear, postfrontal environment. Because of the failure of a second balloon launch at a later time, a single balloon was used to define the Lagrangian trajectory. The balloon signal was acquired successfully from the C-130 during the first and the second flights (flights 18 and 19) but not the third. As a result, the extrapolated trajectory from the last balloon position was used to initiate operations during the third aircraft mission. The air column was traced for a total of about 27 hours (including flight 20).

Figure 2 shows the trajectory of the NCAR C-130. The average location of the circular flight legs is shown as circles, and the average position of the aircraft soundings below 3 km is shown as "plus" symbols. Usually, a sounding is defined as a section of the flight where measurements were made with substantial altitude change. In order to take advantage of the entire measurement set, transits between circles at different levels are also considered soundings, although the vertical coverage of these "mini" soundings was limited. The solid line in Figure 2 is a 6-order polynomial fit to the aircraft trajectory. The starting point, denoted by "asterisk", is a reference point along the trajectory from which curvature distances are calculated and shown as the horizontal distance along the trajectory in the cross-section plots in section 6. Trajectories from other platforms are also shown in this figure. The "cross" symbols denote the location from which soundings from the ECMWF-analyzed fields were extracted at the time of balloon arrival (arrival of the tagged air column). The soundings were interpolated using the boundary layer mean wind along the trajectory. The trajectory of the R/V *Discoverer* is also shown in Figure 2 as a dashed line. The *Discoverer* cruise along the trajectory did not start until 2130 (UTC), December 1, about 9 hours after the release of the balloon. Measurements of sea surface temperature (SST) by the *Discoverer* along this trajectory will be used to calibrate the SST measured by the Heimann radiometer onboard the C-130. Because of the large timescale of SST variation in the ocean, the time lag between the C-130 and the *Discoverer* measurements should not be a problem for the intercomparison of SST measured from the two platforms. Data from the return leg of the *Discoverer* was not used because it deviated considerably from the air column trajectory.

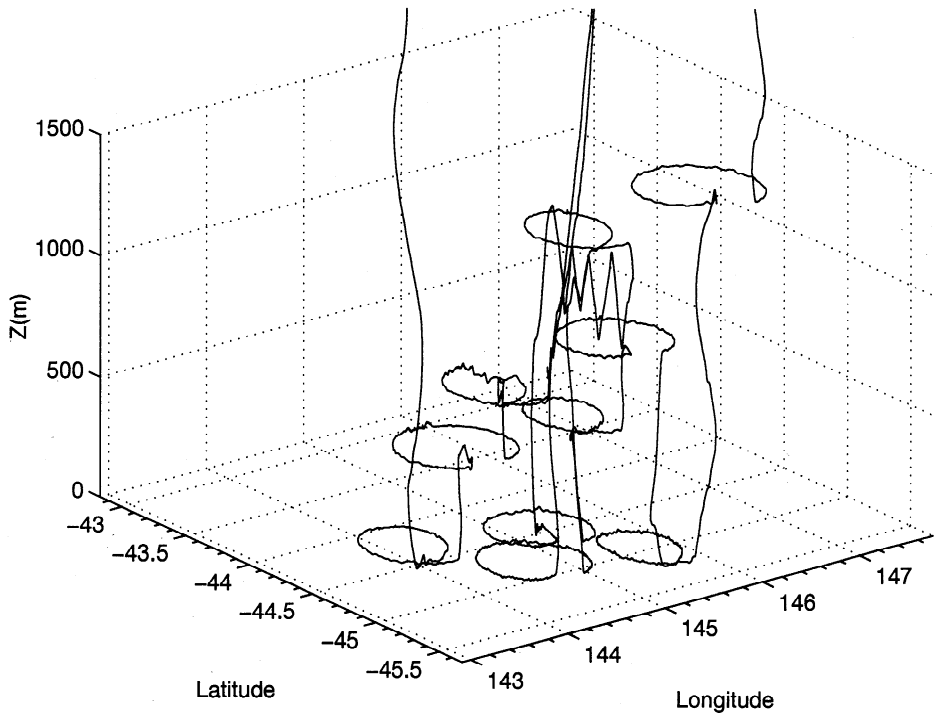

Figure 1. A typical three-dimensional trajectory of the C-130 (from flight 18) measurements in ACE1. Generally, each flight consisted of two vertical stacks of circles 60 km in diameter, two lidar legs across the diameter of the circles at the beginning and the end of the measurement, one or two porpoising legs at the inversion, and two to three full soundings supplemented by multiple minisoundings (transits between level legs at different altitudes). The C-130 was advected by the mean wind at each measurement level during one vertical stack, while it adjusted to a new location centered at the balloon at the beginning of the next stack.

2.2. Lagrangian B

Lagrangian B started with the C-130 (flight 24), making measurements in a large clear patch upwind of the *Discoverer* prior to the first balloon release. Three balloons were launched near (45.6°S, 144.1°E) beginning at 0000 (UTC), December 8, after the first stack of flight 24. Flight 24 continued with two more stacks of circles downwind of the *Discoverer* following the balloon launches. These balloons were monitored for roughly 26 hours during flights 25 and 26. The *Discoverer* departed the Lagrangian launch position at 0100 (UTC), December 9, to sample seawater following the Lagrangian trajectory. Figure 3 shows the trajectories of the Lagrangian flight track, the center balloon (balloon 6), and the R/V *Discoverer*. Locations of the ECMWF soundings are also given in Figure 3.

Lagrangians A and B had very different measurement trajectories. Although they both started in nearly zonal wind, LA had a much stronger westerly wind speed throughout the IOP. In LB, however, the air column had much stronger northerly wind during the second and the third flights, resulting in a southbound trajectory. The measurements of LA extended for approximately 15° longitude and about 7° latitude (starting at 44.4°S, 143°E and ending at 52°S, 158°E), and those of LB were made over 7° longitude and 6° latitude. The maximum distances along the trajectories were about 1500 km and 1000 km for LA and LB, respectively.

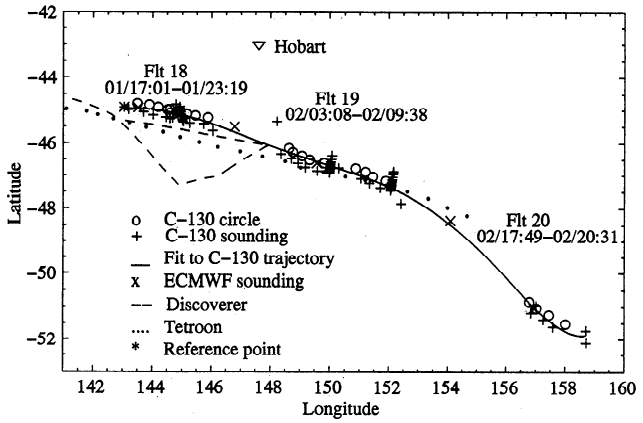

Figure 2. Trajectories of all platforms involved in the Lagrangian A measurements. The mean location of each C-130 circle and sounding are denoted as "circles" and "pluses", respectively. The solid line is a 6-order polynomial fit to the circles and the plus signs. The horizontal axis (in kilometers) in the vertical cross-section plots shown later is based on the curvature distance along this line. The "asterisk" denotes the reference point (44.92°S, 143.05°E) from which the distance was calculated. The dashed line is the trajectory of *Discoverer*; dotted line denotes the balloon trajectory. Locations of the ECMWF soundings are shown in "crosses". The starting and ending date (of December) and times of each flight are also listed at "date/hh:mm." Hobart is denoted by a "▽."

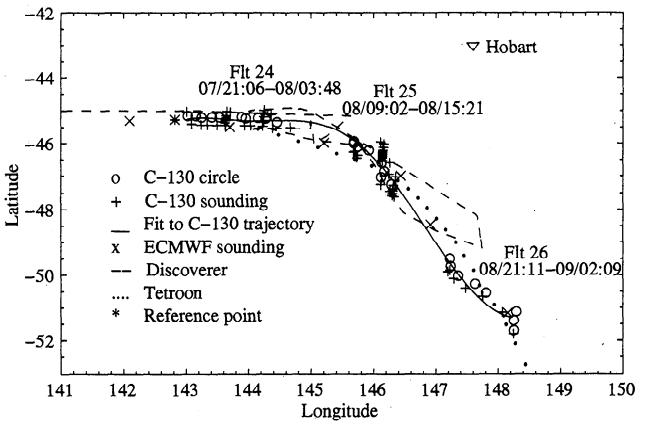

Figure 3. Same as in Figure 2 except for Lagrangian B. Note that three balloons were released and detected during the entire LB measurements; the trajectory of balloon 6 is shown. The reference point (asterisk) is (45.27°S, 142.82°E).

3. An Overview of Synoptic Conditions During LA and LB

Our specific focus here is on how the synoptic meteorology relates to the boundary layer structure. Thorough discussions of the synoptic meteorology may be found in the work of *Businger et al.* [this issue].

The local meteorology at the beginning of both LA and LB held many similarities. The scientific objectives required that the balloons be launched into the middle of a relatively cloud-free boundary layer so that this boundary layer air would remain cloud-free for the duration of the IOP. Observations and theory suggested that the cloud-free air found in postfrontal patterns best met these criteria. Typically, the passage of a cold front is followed with a surge of subsiding colder and drier air from higher latitudes. This subsidence allows only shallow convection to exist, which prevents the formation of deep convective clouds.

During LA the satellite images and mean sea level pressure (MSLP) gradient indicated that the balloon was launched in postfrontal air. At the time of the release, however, the front was far ahead of the long-wave trough, indicating that the front was frontolytic. The balloon was launched near the northern edge of the cold front. The MSLP further reveals that the horizontal winds were nearly zonal at the time of release. Back-trajectory analysis suggested that the air mass had a strong westerly origin with virtually no southerly component. Because the flow was frontolytic, we would not expect the boundary layer to remain cloud-free for an extended period of time. An anticyclone was found over the Australian Bight at this time with weak ridging extending into the postfrontal air mass.

In the ensuing 24 hours, the long-wave trough progressed to the East, while the anticyclone jumps to the east coast of Australia in the Tasman Sea. This anticyclone began to have a greater influence on the boundary layer air, and the air mass gradually took on a more southerly heading. At this stage, the northern edge of the front, near where the balloon was launched, became frontolytic.

The synoptic setting for the start of LB was very similar to that of LA. The balloons were launched behind a weak front, which was far ahead of the long-wave trough. The winds are again nearly zonal. This front did not have a long northern extent. The anticyclone to the North was already located over the Tasman Sea. The evolution of this system, however, was vastly different from that of LA. Over the next 24 hours, a cutoff low crossed the Australian Bight and joined the long-wave trough behind the position of the troughs. The anticyclone over the Tasman Sea began to resemble a blocking pattern. The result of these synoptic developments was that the horizontal winds underwent a major transition from westerly to strong northerly. The air mass had a polar heading and was advecting over continually colder waters. The air column was relatively warm as it was advected to the South and overran a shallow colder air mass. Consequently, cloud layers developed as this relatively warm, moist air ascended.

4. Variations of Sea Surface Temperature

The SST measurement on the C-130 was made by a Heimann radiometer with a manufacturer specified accuracy of ±1°C. It was found, however, by comparing with the SST derived from satellite measurements [*Griffiths et al.*, this issue] that the Heimann might have systematically underestimated the SST. A detailed comparison between the C-130 SST and that measured by the *Discoverer* was therefore carried out for all flights where the two platforms were within a degree in latitude and longitude.

The SST measurement on the NOAA ship *Discoverer* was made with a Seabird SBE-21 thermosalinograph located in the ship's bow, nominally 5 m below the water surface. The thermosalinograph was calibrated by the NW Regional Calibration Facility immediately prior to ACE1. The accuracy of temperature measurements was 0.001°C. The intercomparisons used the C-130 measurements from the lowest-level circular flight legs only in order to minimize the effects of the lower boundary layer air and water vapor on the radiometric SST measurements. It was found, however, that the deviation of the C-130 SST from that of the *Discoverer* varied for each of the Lagrangian cases. Specific calibrations were therefore necessary for each Lagrangian. The calibration was further complicated by the large spatial variation of SST during both Lagrangians, especially in LB. An example of the SST variation is shown in Figure 4b, where the longitudinal variation of SST from part of flight 24 is shown together with the SST measured from the R/V *Discoverer*. The flight track of the C-130 and the trajectory of the *Discoverer* are shown in Figure 4a. Figure 4b shows a longitudinal variation of SST by as much as 3°C along one circular flight path of 60 km in diameter. The *Discoverer* data, measured across the circle, also shows strong variation along each leg and between the two legs. To minimize the uncertainty introduced by spatial variations, only those sections of the measurement where the C-130 was directly over the *Discoverer* path were used for comparison. Consequently, an adjustment of +1.2°C to the C-130 measurements was obtained for LB. Since there was no exact overpass of the C-130 over the *Discoverer* path during LA, sections of the C-130 measurements were isolated when the flight track was the closest to the ship trajectory and compared with the ship measurements. An adjustment of +0.87°C was thus obtained for LA. It should be noted that the adjustment for LA might not be accurate due to the lack of in situ measurements on the same path of the C-130.

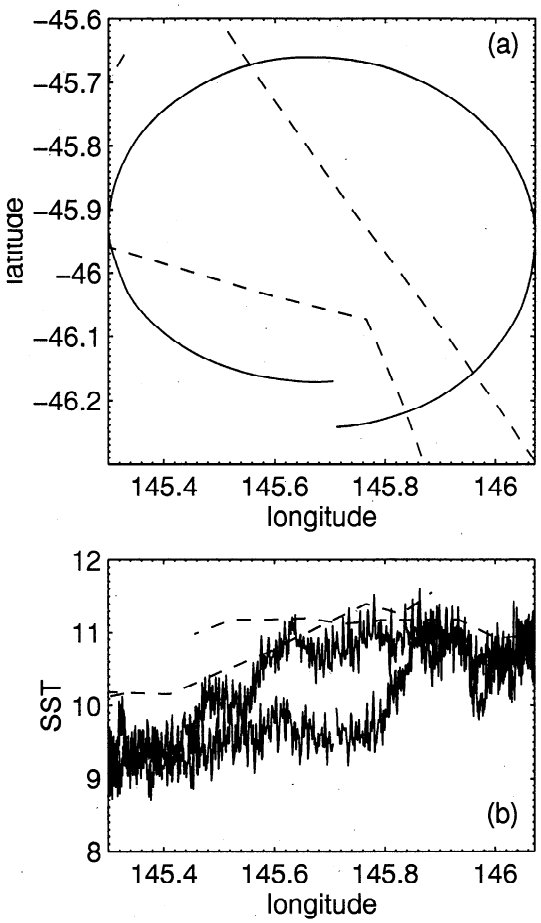

Figure 4. (a) Flight track of a C-130 circle at 50 m above sea level during flight 24 and the *Discoverer* trajectory passing through the vicinity about 40 hours later. (b) Variations of the sea surface temperature observed by the C-130 (uncorrected) and the *Discoverer*. The measurements were made corresponding to the trajectories in Figure 4a. Solid lines: C-130 trajectory and measurement, dashed lines: ship track and measurement.

Unfortunately, we do not have enough supporting data set to estimate the resulting error.

Plate 1 shows the spatial variation of the calibrated SST measured during both Lagrangians. The data were composed from SST measurements from all horizontal flight legs below 500 m. SST measured at different levels below 500 m were compared in order to detect possible effects of the atmosphere on the radiometric SST measurements. No systematic deviations were found, suggesting negligible atmospheric effect on the SST measurements for these levels. Measurements from altitudes higher than 500 m were sometimes above patchy clouds. They are more likely affected by the intervening cloud and therefore are not used for obtaining SST variations. The horizontal projections of all circular flight legs (at all altitudes) from each flight are also shown in these figures.

Although both Lagrangians occurred over subantarctic water (defined as water with salinities between 34.2 and 34.8 practical salinity unit (psu)), the water mass was not uniform, and there were frequent indications of mixing with the subtropical convergence zone waters (salinity > 34.8 psu) to the North and the polar water (salinity < 34.2 psu) to the South [*Bates et al.*, 1998]. The sharp gradients in temperature and salinity in these regions of water mass mixing were evident in the continuous shipboard measurements [*Griffiths et al.*, this issue]. The large variation of SST along each circular flight track is clearly seen in Plate 1, especially from flights 18, 24, and 25. These variations detected by the C-130 are very similar to those derived from satellite remote sensing [*Griffiths et al.*, this issue]. We note that one circular flight leg may fly over very different SST regimes due to the large spatial variation. Since boundary layer turbulence is very sensitive to surface heating/cooling, such variation resulted in significant horizontal inhomogeneity of boundary layer turbulence structure [*Wang et al.*, this issue].

There are substantial similarities in both LA and LB. Both Lagrangians started their first measurement circles in very variable SST regions with increasing SST to the East. As the air column turned toward high latitudes, mean SST decreased, but still with detectable variations. In LB the gradient of SST during the early part of flight 24 and the latter part of flight 25 are both nearly perpendicular to the flight track (the solid SST contour lines in Plate 1b). Consequently, the boundary layer evolution over different regions of SST categorized by *Wang et al.* [this issue] can be considered as the evolution of one air column over various SSTs and synoptic forcing.

5. Variations of Boundary Layer Mean Structure

5.1. Two-Layered Boundary Layer Structure

The general characteristics of the boundary layer and low-level cloud from both Lagrangian measurements are illustrated in Figure 5. The first two flights of LA were made in single-layered boundary layers that were generally well mixed. The base of the main inversion raised considerably on the third flight where the layer below evolved into two layers separated by a weak inversion between 500 m and 700 m. This two-layered structure was persistent throughout Lagrangian B, where a secondary inversion was found between 400 and 600 m above the surface. Figure 6 shows the profiles of potential temperature and water vapor from all soundings during Lagrangian B. The differences in potential temperature and water vapor in the two layers are evident but small compared to that between the air above the main inversion and below. Following the discussions by *Wang et al.* [this issue] and *Russell et al.* [1998], we will refer the lower layer adjacent to the surface as the boundary layer to denote its immediate surface origin. The upper layer will be referred to as a buffer layer to denote its surface origin in its recent history and its detachment from the current surface. In general, the boundary layer was well mixed in both potential temperature and specific humidity, while the buffer layer had stable thermal stratification. *Wang et al.* [this issue] show that the boundary layer was relatively turbulent, while turbulence in the buffer layer was weak and intermittent. The differences between the two layers in other thermodynamic variables are discussed in the following subsections.

5.2. Evolution of the Boundary Layer

The evolution and the thermodynamic properties of the lower troposphere in LA and LB will be described using contour plots from a vertical crosssection along the aircraft

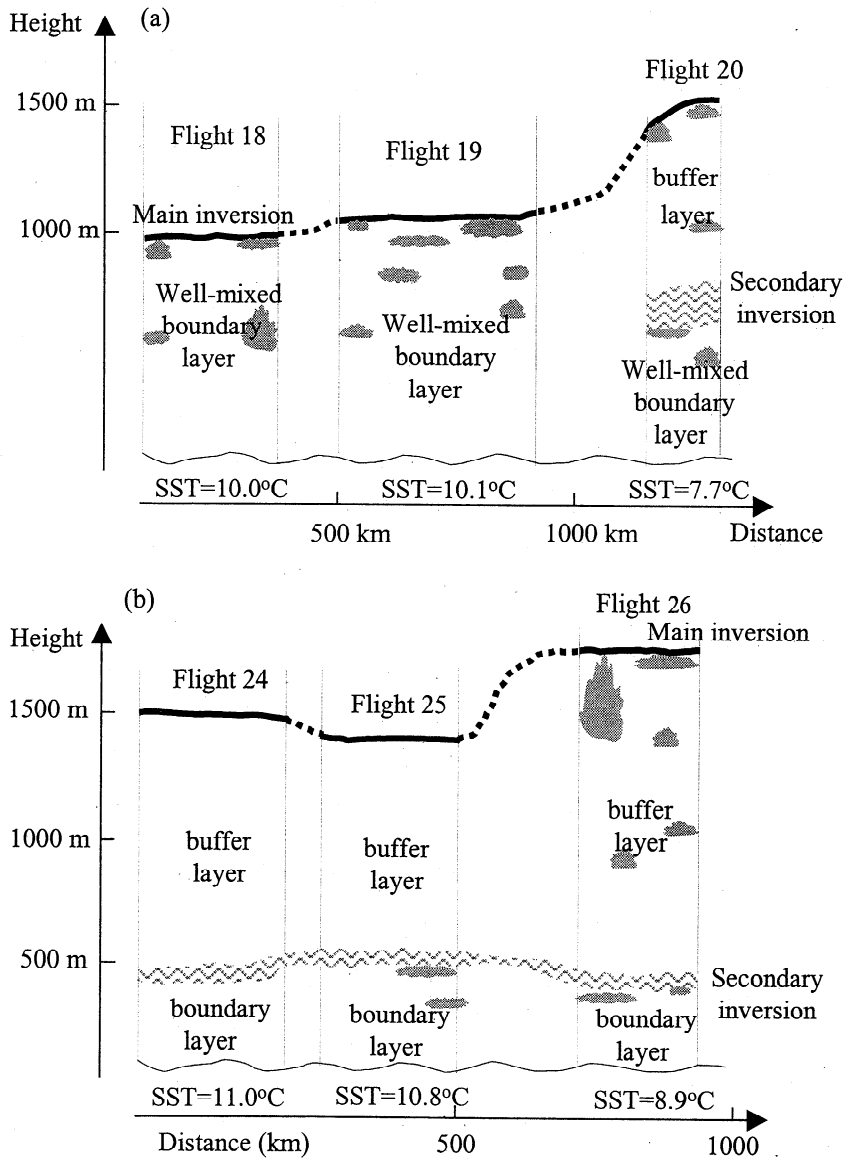

Figure 5. Schematics of boundary layer evolution in (a) Lagrangian A and (b) Lagrangian B.

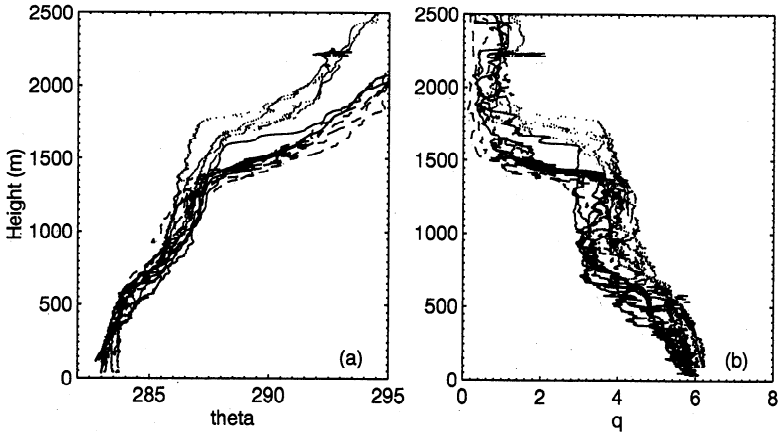

Figure 6. Vertical profiles of (a) potential temperature and (b) specific humidity from aircraft descent/ascent during Lagrangian B. The solid, dashed, and dotted lines are from flights 24, 25, and 26, respectively.

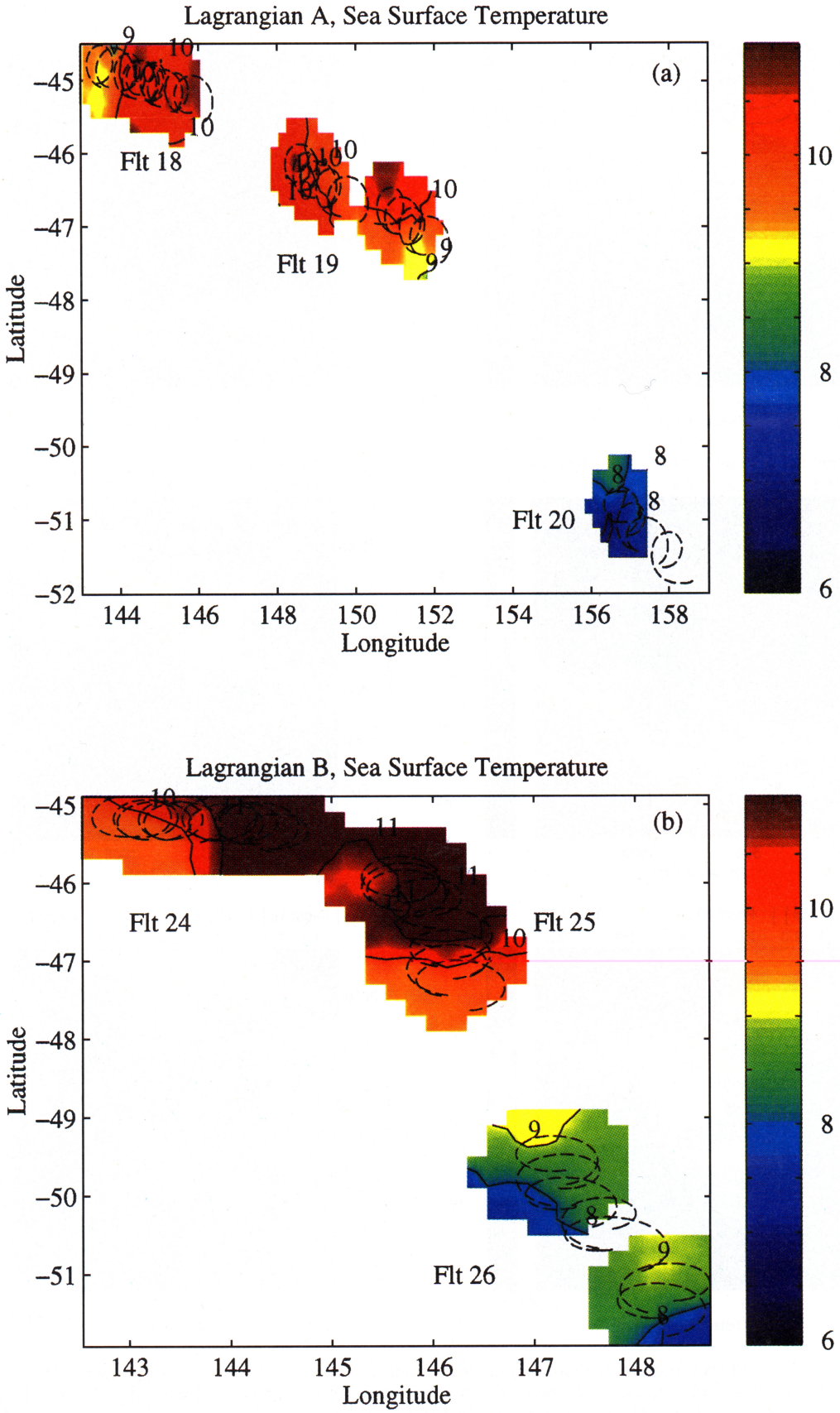

Plate 1. (a) Spatial variation of SST measured by the C-130 during Lagrangian A. The contours are for SST in degree Celsius. A correction of 0.87°C was made to the C-130 measurement. (b) Same as in Plate 1a, except for Lagrangian B. A correction of 1.2°C was made to the C-130 data.

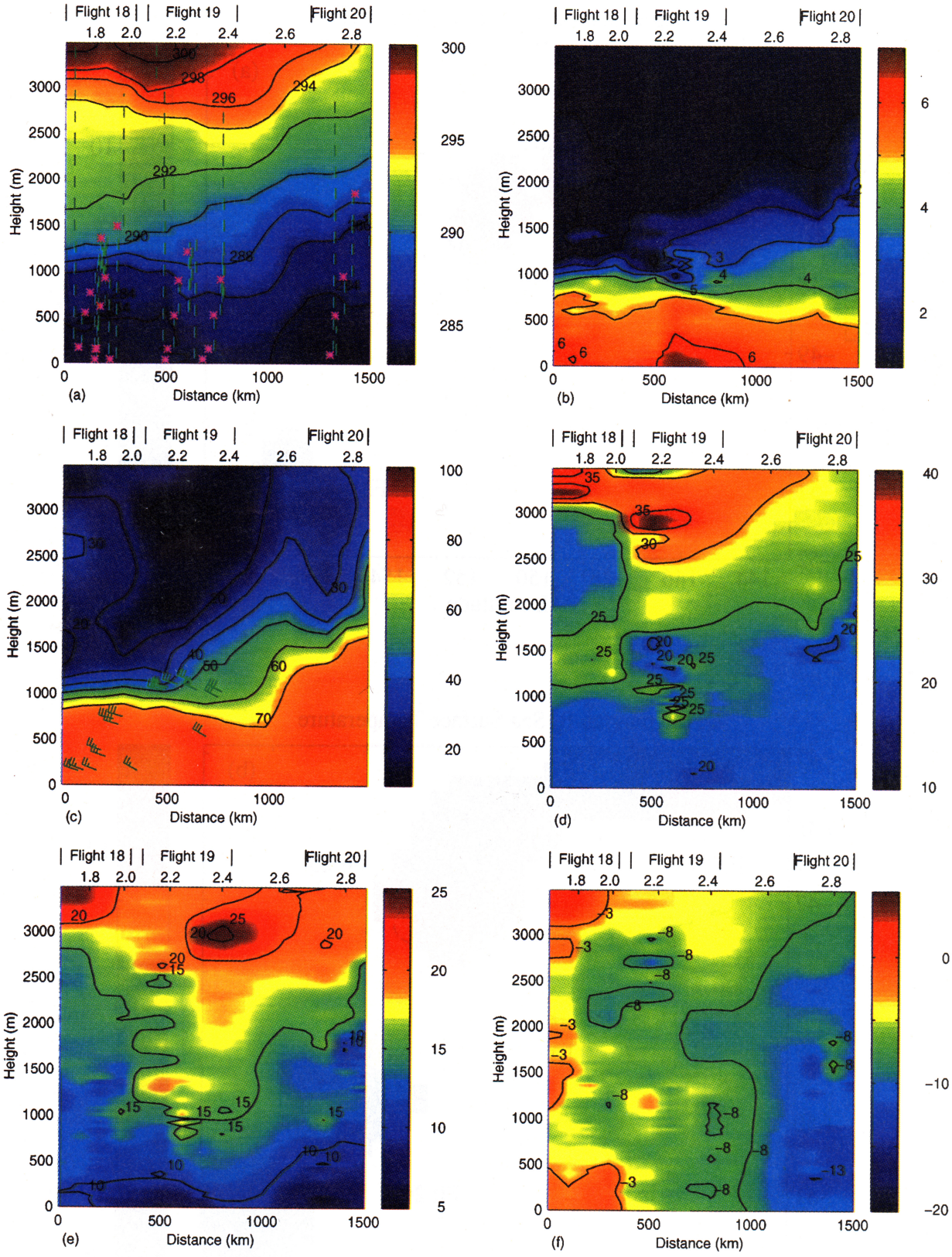

Plate 2. Vertical crosssection of thermodynamics properties observed during LA: (a) potential temperature (K). The location and vertical coverage of the soundings are shown as vertical dashed lines and the mean positions of each circle are shown as "asterisks"; (b) specific humidity in g kg^{-1}; (c) relative humidity; (d) ozone concentration (ppbv); (e) East-West component of horizontal wind (m s^{-1}); and (f) North-South component of horizontal wind (m s^{-1}). Results here were derived from all C-130 soundings and mean values from each circular flight path. The lower horizontal axis is distance along the flight path from the reference point denoted as "asterisk" in Figure 2; the upper horizontal axis is the date in December 1995. Note that the upper axis is not in linear scale.

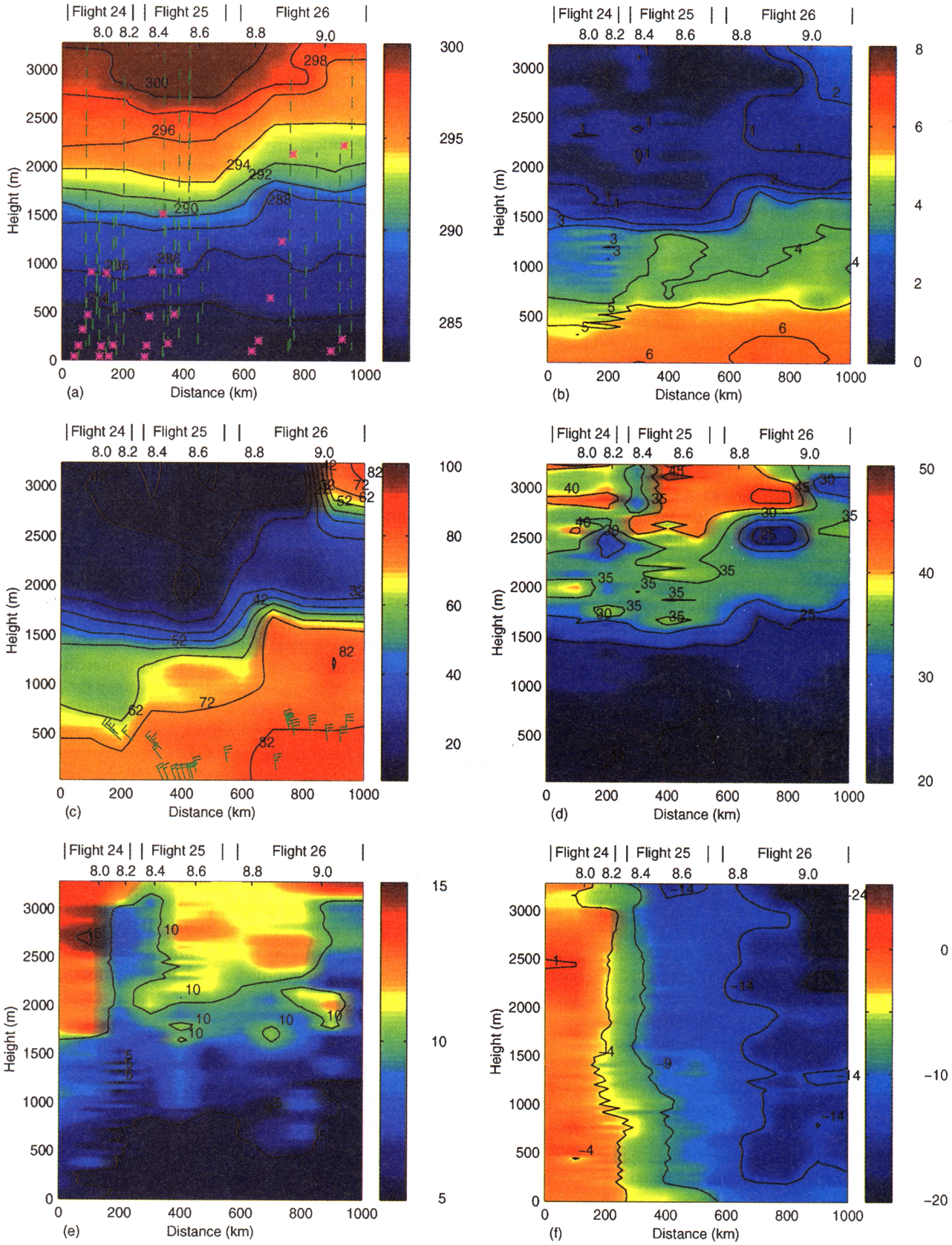

Plate 3. Same as in Plate 2 except for Lagrangian B. The trajectory along which distance is measured and the reference point are shown in Figure 3.

flight track. The data used to generate the cross-section plot include measurements from the descent/ascent soundings and from the leveled circular legs. Since a sounding was generally obtained over some horizontal distance, mean latitude and longitude were obtained to denote an average position of the sounding. This mean position is used to obtain the distance of the sounding along the Lagrangian trajectory (solid line in Figures 2 and 3). If a sounding extended above 3.5 km in altitude, the mean location was calculated using the latitude and longitude below 3.5 km only, since our interests were mainly in the lower troposphere. The mean values from each circle were also input to the cross-section plot.

Evolution of the boundary layer potential temperature, specific humidity, relative humidity, ozone, and horizontal wind components are shown in Plates 2 and 3 for LA and LB, respectively. The vertical dashed lines in Plates 2a and 3a denote the location and the vertical coverage of each sounding used to generate the plot. The "asterisks" are the average locations and altitudes of the circles.

During LA the boundary layer potential temperature (Plate 2a) was well mixed up to about 900 m at $\theta \approx 284$ K on flight 18. Slightly higher temperature was observed on flight 19, especially in the upper boundary layer, and the strength of the inversion decreased. On this flight the upper boundary layer water vapor, ozone, and east-west wind component had a complicated structure. This is possibly associated with local variations of the boundary layer height topped by cloud bands ranging from about 800 m to 1400 m. In general, a temperature inversion, a decrease in specific humidity, and an increase in ozone concentration were observed at the immediate cloud top, which were seen in each individual sounding. These sharp changes in θ, q, and O_3 at different altitudes appear in the contour plot as local anomalies, which is most prominent in the cross section of ozone (Plate 2d).

The vertical shear of the u component was substantial, especially in the lower 400 m of the boundary layer (Plates 2e and 2f). This wind shear was mainly responsible for generating turbulent mixing in the boundary layer [*Wang et al.*, this issue].

Development of the two-layered vertical structure is evident in potential temperature and specific humidity as the air column gradually moved over much colder water on flight 20. The specific humidity (Plate 2b) was, in general, uniform in the boundary layer, while a significant difference is found between the buffer layer and the boundary layer on flight 20. However, relative humidity (Plate 2c) was nearly the same (70-80%) in the buffer layer and the boundary layer.

The two-layered structure is the most prominent feature of the boundary layer in LB, which is evident in the contour plots of θ and q (Plates 3a and 3b). Here specific humidity in the buffer layer was about 1.5-2 g kg^{-1} lower than that in the boundary layer. As the air column moved over a colder sea surface, specific humidity in the boundary layer increased slightly, possibly due to the decreased entrainment rate at the boundary layer top during the last flight [*Wang et al.*, this issue]. In contrast to LA, the relative humidity (Plate 3c) increased in both layers along the LB trajectory. In the boundary layer, RH increased from middle 70% to around 85%. In the buffer layer, RH increased from ~60% in flight 24 to 65-70% in flight 25, and close to 80% in flight 26. Such a large variation in this layer may have a profound influence on aerosol growth.

The difference in ozone concentration between the boundary layer and the buffer layer was evident in the sounding profiles (not shown), although it is not evident on the contour plot (Plate 3d). We found that the buffer layer ozone was, in general, 2-3 ppbv higher than that in the boundary layer. Although this difference is much smaller than that at the main inversion (~7 ppbv or larger), it can be used as a tracer for estimating entrainment rate between the two layers [*Wang et al.*, this issue].

Except near the surface, weak wind shear was found in LB, which is a preferred condition for a successful Lagrangian measurement. In case of weak wind shear the speed of the balloon used to tag the air column would be representative of the speed of the air column, although the altitude of the balloon varied significantly (Plate 3c). The veering of wind from flight 24 to flight 26 is also clearly seen in Plates 3e and 3f.

6. Low-Level Clouds

The cloud structure for both Lagrangians was relatively complex compared to a solid stratocumulus cloud layer. Scattered cloud patches were often observed which had substantial variation in both horizontal and vertical dimensions. We therefore refer to the cloud as cloud bands. The presence of cloud is sketched in Figure 5.

A summary of the cloud coverage and microphysics is given in Tables 1 and 2. These results were obtained from a vertical profile compiled from soundings and horizontal legs from each of the vertical stacks. The letter "a" after the flight number refers to the first stack of that particular flight, while "b" indicates the second stack. Note that since the horizontal flight legs covered only a few distinct altitudes, measurements from the soundings contributed most to the results. This leads to high variability in the composites. To smooth over this variability, we averaged the microphysics measurements over major cloud bands, which have been identified from the composite vertical profiles.

The Particle Measuring Systems (PMS) forward scattering spectrometer probes (FSSP) and 260-X drizzle probe were used for the microphysics observations. The two FSSP probes provided cloud droplet data: the FSSP-300 measured droplets in the radius range of 1.09 - 2.04 μm and the FSSP-100 in the range of 2.875 - 24.5 μm. Drizzle droplets were detected by the 260-X probe, which measured in the range of 38.25 - 514.25 μm.

Table 1. Cloud Conditions and Microphysics Properties from Soundings and Level Legs of Lagrangian A

Flt	P, hPa	F_{cloud}	N cm^{-3}	LWC g kg^{-1}	r_e, μm		Drz Flux
					Max	Ave	
18a	960-850	0.20	70	0.10	14.0	8.0	0.03
18b	950-840	0.25	70	0.20	14.0	8.0	0.15
19a	950-850	0.20	50	0.10	13.0	7.5	1.75
19b	950-890	0.10	40	0.05	9.0	7.0	0.00
20	970-800	0.20	85	0.10	13.5	8.0	0.00

N is the number concentration, LWC is the liquid water content, both are averaged for in-cloud measurement only; r_e is the effective radius from FSSP; and F_{cloud} is the cloud fraction. The "a" and "b" for each flight denote that the measurements were made during the first and second vertical stacks of measurements, respectively. Drizzle flux (Drz, mm day^{-1}) is averaged for all time.

Table 2. Same as in Table 1 except for Lagrangian B

Flt	P, hPa	F_{cloud}	N cm^{-3}	LWC g kg^{-1}	r_e, μm Max	r_e, μm Ave	Drz Flux
25b	955-905	0.10	75	0.10	10.5	7.5	0.03
26a	990-920	0.20	50	0.10	9.5	5.5	0.15
	850-800	0.40	50	0.06	8.0	7.5	1.75
26b	980-920	0.35	50	0.02	5.5	5.0	0.00
	880-800	0.10	65	0.05	11.0	8.0	0.05

During LA the low-level clouds were observed to resemble scattered cumulus as well as broken stratocumulus. Overall, the fractional cloud cover was lower than 25%. The cloud top and base were not well defined and the soundings showed subadiabatic liquid water content (LWC). The table includes the average droplet concentration and the resulting LWC, where the average was done for the in-cloud sections only. The number concentration was low, between 40 and 85 cm^{-3}. The average effective radius through the layer was calculated to be 8 μm with a maximum of approximately 14 μm. The drizzle flux (averaged for all times) was also extremely weak.

Strong north-south gradients in cloud fraction were observed during the first stack of flight 19. The observers on the flight indicated that the C-130 was flying across a front. The northern edge of the flight circles consistently entered a rather solid cloud band. Similarly, the satellite imagery shows the remains of a front with a nearly west-east orientation. During this stack, large drizzle flux was recorded toward the top of the cloud layer (Table 1, stack 19a). It is possible, however, that this large value was an artifact of the presence of ice that resulted in a relatively small number of large drops recorded by the 260-X probe.

Cloud bands were observed both in the boundary layer and in the buffer layer on flight 20. The measurement between 970 and 800 hPa was averaged to obtain a composite profile and the cloud microphysics quantities (Table 1, bottom row). The presence of a strong north-south gradient in cloud cover was not evident from the measurement.

Flight 24 of LB was essentially cloud-free and thus excluded from Table 2. Flight 25 occurred as the trajectory began to undertake a strong southerly heading. The first stack of flight 25 was also excluded due to the small cloud fraction (~2%). During the second stack (25b), the fractional cloud cover increased to around 10%. Cloud was encountered at the southern part of the circles at two measurement levels (955 and 905 hPa).

The final flight of Lagrangian B, however, demonstrated very complicated cloud microphysics. As the air moved farther south, condensation appeared to occur as a result of increasingly cold air temperature. Two major bands of cloud at different levels were observed throughout flight 26, one in the boundary layer air, one in the buffer layer. Cloud fraction ranged from 10% to 40%.

Compared to measurements in nearly solid stratocumulus cloud in midlatitude [*Nicholls*, 1984], the cloud observed during the Lagrangian measurements of ACE1 is not only complicated and variable but also small in number concentration. Nicholls observed a mean droplet number concentration of about 150 N cm^{-3}. He also found that cloud liquid water content generally followed the adiabatic liquid water content, which is not observed in the cases here. Because of the stable environment and the scattered nature of the cloud bands, the characteristics of turbulence mixing and cloud microphysics may be significantly different in the cloud bands compared to those presented by *Nicholls* [1984] or other stratocumulus cases. However, as we will see in the work of *Wang et al.* [this issue], the cloud bands indeed generated turbulence mixing in an otherwise stably stratified buffer layer environment.

7. Inversion Structure and the Role of Large-Scale Forcing

We illustrate here the role of large-scale ascent/descent in determining the boundary layer and inversion structure along the Lagrangian trajectories. The divergence/convergence along the flight tracks by the ECMWF analyses are shown in Figures 7a and 8a for both Lagrangians. The subsidence/ascent velocity (Figures 7b and 8b) was obtained by vertically integrating the divergence/convergence field. Here the horizontal axis denotes the distance along the trajectory from a reference point (denoted as an "asterisk" at the beginning of the flight track in Figures 2 and 3). The locations of soundings from the ECMWF analyses are shown as crosses in Figures 2 and 3.

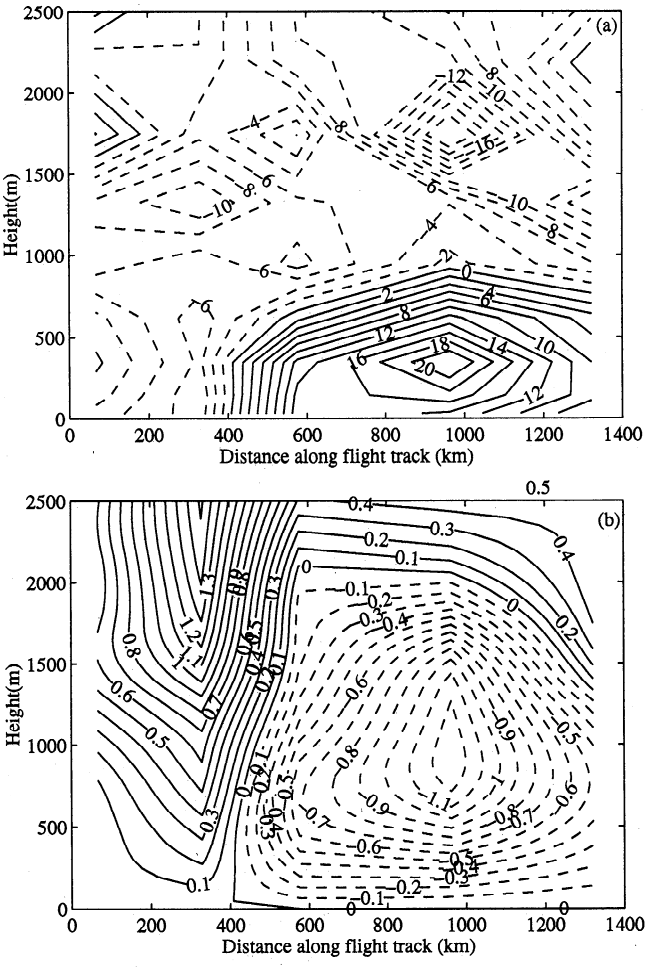

Figure 7. (a) Analyzed field of large-scale convergence and divergence from ECMWF. The *Discoverer* soundings were assimilated into the ECMWF analyses. The values are shown in 10^{-6} s^{-1}. (b) Large-scale ascent/subsidence velocity (cm s^{-1}) integrated from the convergence/divergence field.

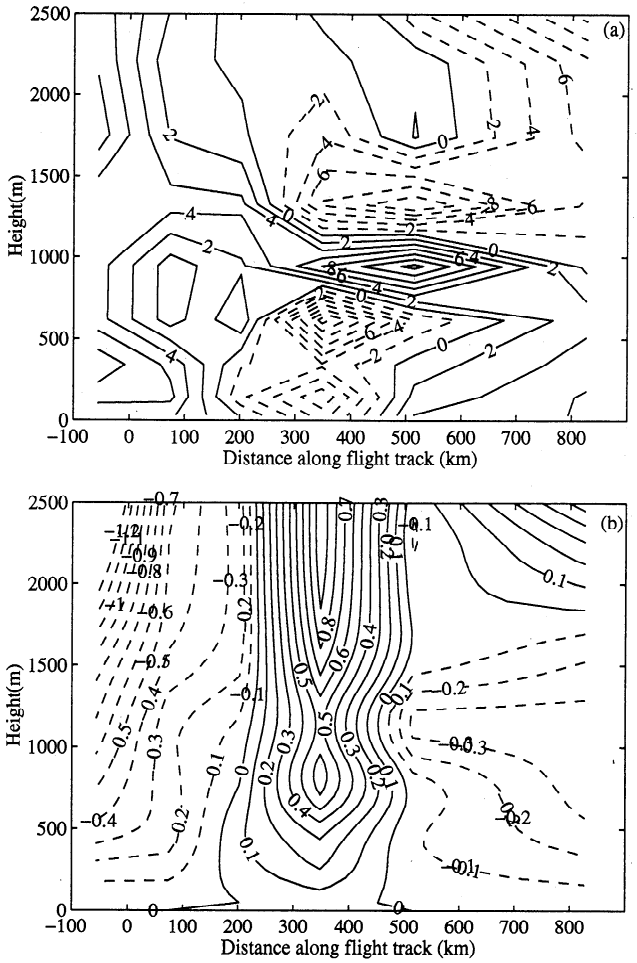

Figure 8. Same as in Figure 7 except for Lagrangian B.

The divergence/convergence fields showed strong temporal/spatial variability during both Lagrangians. In particular, we found strong vertical variations of divergence in the lower 3 km of the troposphere. LA started in a large-scale convergent flow (and therefore ascent velocity) just behind the weakening front. It shows in Figure 7b that the boundary layer was in slow ascent in the first 400 km along the trajectory. At the end of flight 19, ECMWF showed divergent flow in the lower boundary layer below 900 m. Maximum descent velocity of -1.2 cm s^{-1} was found at 1 km altitude at nominally 950 km downstream of the LA trajectory.

LB started in the postfrontal subsidence air in the boundary layer and above. During flight 24, subsidence velocity below 500 m averaged to about -0.15 cm s^{-1}. On flight 25, ECMWF showed general ascent with a maximum ascent velocity of 0.6 cm s^{-1} at about 800 m above the surface and another maximum ascent velocity at about 2500 m above sea level. On flight 26, low-level divergence and subsidence again prevailed below 1 km.

It is desirable to discuss the validity of the ECMWF-analyzed large-scale fields. For this purpose we will first examine the ECMWF-analyzed potential temperature and specific humidity fields (Figures 9 and 10) and compare them with the aircraft direct measurements shown in Plates 2 and 3. In general, the ECMWF-analyzed fields were able to reproduce the major features in the observations, especially in potential temperature and specific humidity in the free troposphere (compare Plates 2a and Figure 9a, Plate 3a and Figure 10a). The evolutions of the buffer layer in LA and in LB were also reproduced by ECMWF. We also found the increase of the buffer layer depth in LB during flight 26 as well as the decreased vertical gradient in potential temperature in the lower buffer layer, which are consistent with the observations. Since the free troposphere was basically laminar flow and the buffer layer had very weak turbulence, the temperature and water vapor structure in these layers were largely determined by large-scale environment. The consistency between the observed and the analyzed scalar fields suggested that the ECMWF divergence field was diagnosed reasonably well. *Suhre et al.* [1998] found, using a one-dimensional (1-D) turbulence closure model, that the temperature structure above the boundary layer was very sensitive to the large-scale vertical velocity. They also found that the ECMWF-analyzed vertical velocity field resulted in very similar inversion structure in their model as well as in the C-130 observations. Nevertheless, because of the large spatial resolution of the ECMWF-analyzed field (a nominal 250 km), we should not expect high accuracy divergence fields on scales less than the length scale of model resolution.

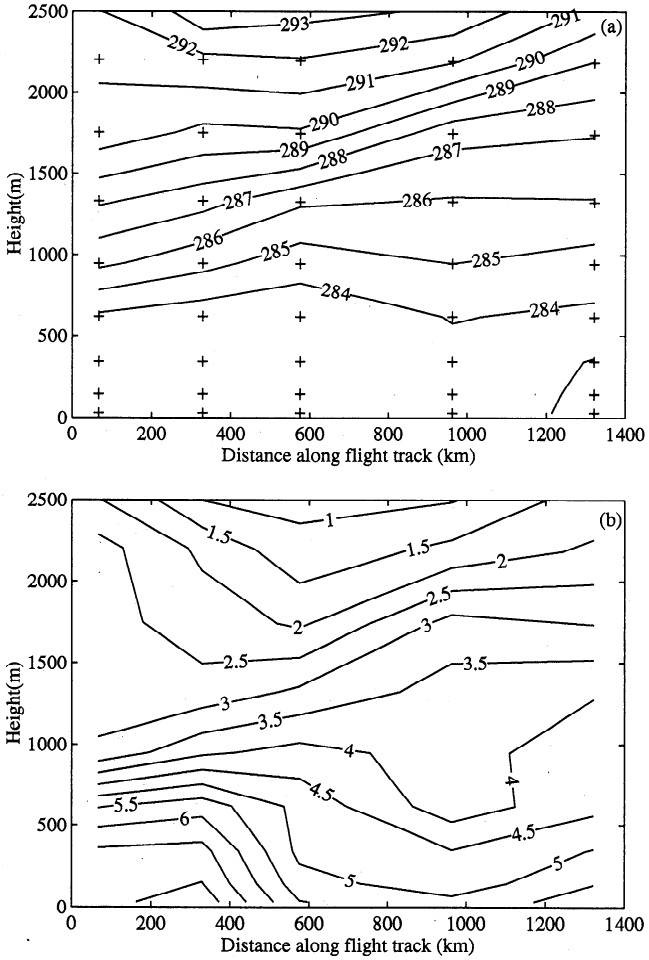

Figure 9. Vertical cross sections along the Lagrangian A trajectory from ECMWF analyses: (a) potential temperature field, (b) water vapor specific humidity field.

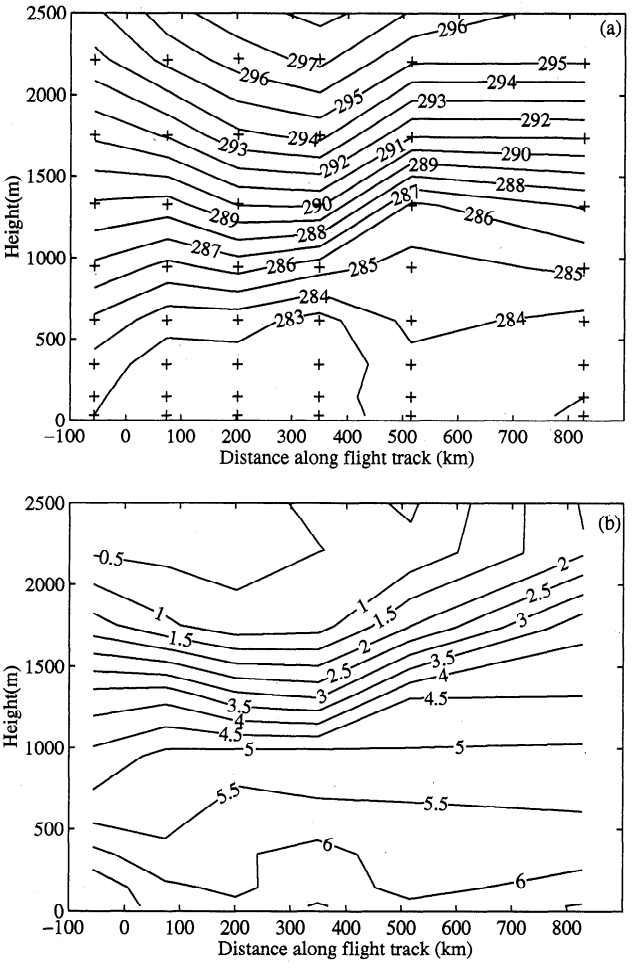

Figure 10. Same as in Figure 9 except for Lagrangian B.

We also obtained direct measurements of divergence and mean vertical motion computed from the component of the wind normal to the circular flight path of the C-130 integrated around the circles of about 60 km in diameter. The technique is described by *Lenschow* [1996]. For LA the divergence as a function of height was obtained by a least squares linear fit to the closed integrated around the circular flight patterns at the sequential levels. The levels and the results are given in Table 3.

The mean vertical motion at height z is the negative of the integral of div from the surface to z, with the assumption of zero vertical motion at the surface. For flight 18 the vertical motion decreases with height down to about -0.2 cm s^{-1} at about a kilometer, then increases above that level, crossing zero at about 2.3 km height. For flight 19 the resulting mean vertical motion gives a slightly positive mean vertical motion that peaks at about 0.02 cm s^{-1} at about 80 m, decreases to zero at about 160 m, and continues to decrease above this level. Only two levels of circles were available for flight 20; the divergence estimate in Table 3 gives a positive mean vertical motion that increases linearly with height; at 460 m the mean vertical motion is about 0.2 cm s^{-1}.

ECMWF and the direct aircraft measurements resolved the divergence field at two different scales. We noted some differences between the two estimates. For LA, ECMWF predicts upward motion over the first 400 km of the trajectory, which does not agree well with the measured downward motion in the lowest 2 km during flight 18. The aircraft-measured divergence field appeared to be consistent with the pronounced inversion and relatively constant inversion height. The ECMWF predicts downward motion during flight 19, which agrees with the measurements. During flight 20 the ECMWF predicts a small downward motion with a rather large increase with time. The measurements are limited but show a positive mean vertical motion. We emphasize, though, that the aircraft measurements covered a much smaller area than ECMWF grid resolution. As a result, the aircraft direct estimate may include possible mesoscale variations, and we do not expect the two results to be the same.

For LB the divergences were estimated by *Russell et al.* [1998] from the circular flight patterns and used to estimate the entrainment velocity at the top of the boundary layer. Their divergence estimates for the boundary layer and the buffer layer, respectively, are as follows: for flight 24, 5.9×10^{-5} s^{-1} and 1.8×10^{-6} s^{-1}; for flight 25, 2.7×10^{-5} s^{-1} and 1.8×10^{-5} s^{-1}; and for flight 26, -8.9×10^{-5} s^{-1} and 3.5×10^{-5} s^{-1}. In comparison with the ECMWF vertical motion, both results show downward vertical velocity during the period of the first fight. The ECMWF predicts upward motion, and the measurements show downward motion during flight 25. During flight 26 the ECMWF predicts downward motion below 1700 m and upward motion above, while the airplane measured upward motion throughout the boundary layer decreasing to almost zero at the top of the buffer layer during flight 26. On the basis of this and the observed increase in the height of the buffer layer top with time, the ECMWF seems to predict too strong an upward motion in the 200 to 400 km distance region. In fact, the upward motion seems to actually occur slightly farther along the trajectory.

8. Discussion

We will discuss the likelihood of following one air column during each Lagrangian in ACE1. This question is essential to the budget analysis from the Lagrangian measurements. If the same air mass was not followed throughout the measurements, the budget equation has to include the effects of horizontal advection, a component of the Eulerian budget

Table 3. Divergence Estimates From Circular Measurements of Lagrangian A

Flight	Altitudes of All Circles Involved, m	Divergence, s^{-1}
18	150, 550, 760, 30, 1400, 150, 610, 910, 30, and 1520	$div = -0.32 \times 10^{-8}z + 0.37 \times 10^{-5}$
19	30, 150, 520, 910, 30, 150, 520, and 910	$div = 0.68 \times 10^{-7}z + 0.54 \times 10^{-5}$
20	30, 460	$div = -0.43 \times 10^{-5}$

Here, z is altitude in meters.

equation that is difficult to measure accurately. A complete answer to this question requires detailed back-trajectory analysis from the large-scale wind field, a subject to be addressed by *Businger et al.* [this issue]. The discussion here is based on the observed wind field.

We believe that the Lagrangian philosophy was successfully fulfilled in LB. This is first supported by the fact that vertical variations in wind speed and direction were relatively small (Plates 3e and 3f) except on the last flight (flight 26). The speed of the balloon was therefore insensitive to its variation in altitudes (shown in Plate 3c). Secondly, the upper air temperature and water vapor evolved rather smoothly throughout LB (Plates 3a and 3b), suggesting that the upper air was likely air mass of the same origin. Finally, all three balloons were followed until the last flight without significant dispersion in positions [*Businger et al.*, this issue], suggesting that the wind field did not have significant spatial variability, an ideal condition for Lagrangian measurements.

The conditions in LA were not so favorable for Lagrangian measurements as in LB due to the increased wind shear. On flight 18 the largest wind shear was found in the lowest 750 m, where the mean wind speed increased from 10 m s^{-1} to about 14.5 m s^{-1}, and the wind direction changed from 280° to about 290°. If we assume that the air column started at the beginning of flight 18, the wind shear would have resulted in a distance of about 187 km between the surface air and the air at the boundary layer top at the beginning of flight 19. Similar magnitude of wind shear was also observed on flights 19 and 20. We estimated that the maximum possible deviation of the top of the boundary layer from the surface air was nominally 700 km due to the observed vertical shear. This deviation is fairly large compared to the diameter of the measurements circle but is still less than the scale of air mass variation in general synoptic disturbances. We also noted that the altitude of the balloon varied considerably during LA (Plate 2c). In flight 18 the mean altitude of the balloon was about 369 m in the nearly 1 km deep boundary layer, moving at a mean speed of 14.7 m s^{-1} at a direction of 288°. On flight 19 the balloon was found above the boundary layer with an indicated mean altitude of 985 m and a nearly constant speed of 15.6 m s^{-1} and direction of 291° (Plate 2c). The boundary layer mean wind was 14 m s^{-1} at 300°. The mean balloon speed during the first two flights seems to be reasonably close to the wind averaged over the entire boundary layer. Since the balloon signal was lost on the third flight of LA, flight 20 followed the extrapolated trajectory of the last balloon position. Assuming an error of 5 ms^{-1} in the extrapolated velocity (a nominal 30% error for a wind speed of 15 ms^{-1}), the deviation of the aircraft position from the true airmass location would be ~50 km during the last flight. This deviation is smaller than the diameter of a circle. In conclusion, the vertical shear of boundary layer wind may have resulted in substantial separation of layers at different altitudes of the air column at the start of LA. However, the scale of separation was still smaller than the typical length scale of airmass modification. A budget analysis is still possible if the airmass was relatively homogeneous. In addition, it is shown by *Wang et al.* [this issue] that turbulence mixing in the boundary layer was relatively homogeneous due to turbulent mixing by strong wind shear. Therefore horizontal advection of aerosol and chemical species may not seriously affect their budget in the event that a single air column was not strictly followed. Nevertheless, an in-depth evaluation of the role of horizontal advection should be done before any budget study using data from this Lagrangian measurement.

9. Summary and Conclusions

Observations from six flights made by the NCAR C-130 during two Lagrangian measurement periods are analyzed in addition to ship measurements of SST and the ECMWF analyses. The purpose of this study is to characterize the marine boundary layer environment and the evolution of the mean boundary layer and inversion layer structure.

It is found that the air columns in both Lagrangians went through an ocean surface with substantial variation in sea surface temperature and experienced complicated large-scale dynamical environment. The most variation of SST was found during the first and the second flight of each Lagrangian at around 45°S where an ocean front existed. We also found that corrections of +0.87 °C for LA and +1.2 °C for LB to the radiometric SST measurements were necessary. These corrections were obtained by comparing with the in situ SST measurements from the R/V *Discoverer*.

Both Lagrangian intensive observations started in nearly zonal wind of moderate magnitude. The north-south wind component quickly increased during the second flight and the maximum wind speed was as large as 20 ms^{-1} during the last flight of LA and about 15 ms^{-1} during the last flight of LB. However, LA went through a much longer trajectory due to its extraordinarily strong wind.

The most prominent feature of the Lagrangian cases was the two-layered structure in the boundary layer observed during the last flight of LA and throughout LB. The two layers had distinct differences in potential temperature, specific humidity, and ozone concentration. The buffer layer was topped by a strong inversion with very low water vapor content (<1 g kg^{-1}, RH 20%) aloft. Substantial differences in water vapor were also found between the boundary layer and the buffer layer. This difference can be used to denote the amount of mixing between the two layers discussed by *Wang et al.* [this issue].

Both Lagrangians also started in postfrontal air. Clouds were observed in all flights of LA and in the last two flights of LB with complicated vertical and horizontal structure. As a result, the observed clouds are referred to as cloud bands rather than cloud layers. The cloud bands were generally low in number concentration (less than 80 cm^{-3}) and had lower liquid water content (< 0.20 g kg^{-1}) compared to stratocumulus clouds in midlatitude and subtropical latitudes. In LA, as the tagged air column was fairly close to a front, the cloud had more convective appearance that closely resembled cumulus rather than layered clouds. Midlevel clouds were observed in both Lagrangians which may affect solar radiation into the lower boundary layer.

The large-scale subsidence/ascent velocity from ECMWF analyses showed large variability of large-scale environment as the frontal systems evolved. The time and vertical variation of large-scale vertical velocity play a significant role in modifying the inversion and the boundary layer structure. ECMWF-analyzed potential temperature and specific humidity fields show significant similarity with the aircraft observations, suggesting that ECMWF-analyzed fields worked reasonably well in the ACE1 region. We found some

differences between the ECMWF divergence field and the aircraft direct measurements from the circles. These differences are expected since the aircraft measurements covered a much smaller area than the ECMWF-resolved field.

Acknowledgments. This research is a contribution to the International Global Atmospheric Chemistry (IGAC) core project of the International Geosphere-Biosphere Program (IGBP) and is part of the IGAC Aerosol Characterization Experiment (ACE). We gratefully acknowledge the rapid access to all ACE1 data via the UCAR office. Comments from the reviewers are extremely helpful in improving the manuscript and are highly appreciated. Part of Q. Wang and L. Pan's work was sponsored by the National Science Foundation grant ATM-9700845. Q. Wang's participation in ACE1 field experiment and the initial analysis of ACE1 data were sponsored by the Research Initiative Program (RIP) at the Naval Postgraduate School. The National Center for Atmospheric Research is sponsored by the National Science Foundation.

References

Bates, T. S., B. J. Huebert, J. L. Gras, B. Griffiths, and P. A. Durkee, The International Global Atmospheric Chemistry (IGAC) project's first Aerosol Characterization Experiment (ACE1): Overview, *J. Geophys. Res.*, *103*, 16,297-16,318, 1998.

Bretherton, C. S., P. Austin, and S. T. Siems, Cloudiness and marine boundary layer dynamics in the ASTEX Lagrangian Experiment, II, Cloudiness, drizzle, surface fluxes, and entrainment. *J. Atmos. Sci.*, *52*, 2724-2735, 1995.

Businger, S., R. Johnson, J. Katzfey, S. Siems, and Q. Wang, Smart tetroons for Lagrangian airmass tracking during ACE1, *J. Geophys. Res.*, this issue.

Griffiths, F. B., T. S. Bates, P. K. Quinn, and R. Greene, Descriptive physical, chemical, and biological oceanography of the ACE1 experiment area. *J. Geophys. Res.*, this issue.

Huebert, B. J., A. Pszenny, and B. Blomquist, The ASTEX/MAGE experiment, *J. Geophys. Res.*, *101*, 4319-4329, 1996.

Lenschow, D.H., A proposal for measuring entrainment into the cloud-capped boundary layer, in *Proceedings of the Workshop on Cloud Process Modeling and Measurement*, edited by A.S. Frisch, D.A. Randall, and W.H. Schubert, Colo. State Univ., and NOAA/ETL, Boulder, Colo., 1996.

Nicholls, S., The dynamics of stratocumulus: Aircraft observations and comparisons with a mixed layer model, *Q. J. R. Meteorol. Soc.*, *110*, 783-820, 1984.

DE Roode, Stephen R., and P. G. Duynkerke, 1997: Observed Lagrangian transition of stratocumulus into cumulus during ASTEX: Mean state and turbulence structure, *J. Atmos. Sci.*, *54*, 2157-2173.

Russell, L.M., D.H. Lenschow, K.K. Laursen, P.B. Krummel, S.T. Siems, A.R. Bandy, D. Thornton, and T. S. Bates, Bidirectional mixing in an ACE1 marine boundary layer overlain by a second turbulent layer, *J. Geophys. Res.*, *103*, 16,411-16,432, 1998.

Suhre, K., C. Mari, T.S. Bates, J.E. Johnson, R. Rosset, Q. Wang, A.R. Bandy, D.R. Blake, F.L.Eisele, G.L. Kok, R. L. Mauldin III, A. Prévot, R. D. Schillawski, D. C. Thornton, Physicochemical modeling of ACE-1 Lagrangian B, 1, A moving column approach, *J. Geophys. Res.*, *103*, 16,433-16,455, 1998.

Wang, Q., Boundary layer turbulence structure observed during the Lagrangian measurements in ASTEX, in *Proceedings of the Workshop on Cloud Process Modeling and Measurement*, edited by A.S. Frisch, D.A. Randall, and W.H. Schubert, Colo. State Univ., and NOAA/ETL, Boulder, Colo., 1996.

Wang, Q., D. H. Lenschow, L. Pan, R. D. Schillawski, G. L. Kok, A. S. H. Prévot, K. Laursen, L. M. Russell, A. Bandy, D. Thornton, and K. Suhre, Characteristics of the marine boundary layers during two Lagrangian measurement periods, 2, Turbulence structure, *J. Geophys. Res.*, this issue.

Zhuang, L., and B. J. Huebert, A Lagrangian analysis of the total ammonia budget during the Atlantic Stratocumulus Transition Experiment/Marine Aerosol and Gas Exchange, *J. Geophys. Res.*, *101*, 4341-4350, 1996.

T. S. Bates and J. E. Johnson, NOAA/PMEL, 7600 Sand Point Way NE, Seattle, WA 98115.

S. Businger and B. J. Heubert, Department of Oceanography, University of Hawaii, Honolulu, HI 96826.

G. L. Kok, A. S. H. Prévot, and R. D. Schillawski, NCAR/RAF, Boulder, CO 80307.

P. Krummel, CSIRO DAR, Private mailbag 1, Aspendale, Victoria 3195, Australia.

D. H. Lenschow, NCAR/MMM, Boulder, CO 80307.

L. Pan, Meteorology Department, University of Hawaii, Honolulu, HI 96826.

S. Siems, Department of Mathematics, Monash University, Clayton, Victoria 3168, Australia.

K. Suhre, Laboratorie d'Aérologie, UMR CNRS/UPS 5560, 31400 Toulouse, France.

Q. Wang, Meteorology Department, Naval Postgraduate School, Monterey, CA 93943.

(Received January 26, 1998; revised October 14, 1998; accepted December 14, 1998.)